RESEARCH ARTICLE

Closed-Loop Feedback Control of a Continuous Pharmaceutical Tablet Manufacturing Process via Wet Granulation

**Ravendra Singh · Dana Barrasso · Anwesha Chaudhury ·
Maitraye Sen · Marianthi Ierapetritou · Rohit Ramachandran**

Abstract The wet granulation route of tablet manufacturing in a pharmaceutical manufacturing process is very common due to its numerous processing advantages such as enhanced powder flow and decreased segregation. However, this route is still operated in batch mode with little (if any) usage of an automatic control system. Tablet manufacturing via wet granulation, integrated with online/inline real time sensors and coupled with an automatic feedback control system, is highly desired for the transition of the pharmaceutical industry toward quality by design as opposed to quality by testing. In this manuscript, an efficient, plant-wide control strategy for an integrated continuous pharmaceutical tablet manufacturing process via wet granulation has been designed in silico. An effective controller parameter tuning strategy involving an integral of time absolute error method coupled with an optimization strategy has been used. The designed control system has been implemented in a flowsheet model that was simulated in gPROMS (Process System Enterprise) to evaluate its performance. The ability of the control system to reject the unknown disturbances and track the set point has been analyzed. Advanced techniques such as anti-windup and scale-up factor have been used to improve controller performance. Results demonstrate enhanced achievement of critical quality attributes under closed-loop operation, thus illustrating the potential of closed-loop feedback control in improving pharmaceutical tablet manufacturing operations.

Nomenclature

A	Surface area (in square meters)
C_{API}	API composition (–)
d_{50}	Mean particle size (in meters)
F	PBM density function particles
H	Height (in meters)
m	Mass (in kilograms)
n	Number (–)
P	Compaction pressure (in megapascals)
R	Radius (in meters)
RSD	Relative standard deviation (–)
RT	Residence time (in seconds)
ε	Porosity (–)
ρ_{bulk}	Powder bulk density (in kilograms per cubic meter)
σ	Material stress (in megapascals)
$\mathscr{R}$	Rate (in particles per second)
ω	Feeder rotation rate (in revolutions per minute)
k_{break}	Breakage kernel
K^{rc}	Stress-angle empirical parameter
θ	Delay
τ	Time constant

Domain

g	Gas
n	Component
r	Particle size
s_1	API
s_2	Excipient

R. Singh · D. Barrasso · A. Chaudhury · M. Sen · M. Ierapetritou · R. Ramachandran (✉)
Engineering Research Center for Structured Organic Particulate Systems (ERC-SOPS), Department of Chemical and Biochemical Engineering, Rutgers, The State University of New Jersey, Piscataway, NJ 08854, USA
e-mail: rohit.r@rutgers.edu

R. Singh
e-mail: ravendra.singh@rutgers.edu

z_1 Axial
z_2 Radial

Subscript

in   Inlet stream
out   Outlet stream
P   Pressure
sp   Set point
ω   Rotation rate

Superscript

disc Feed frame disk
f   Feeder
ff   Feed frame
m   Mixer
mil   Mill
tp   Tablet press

Introduction

The pharmaceutical industry is currently under pressure to introduce innovative manufacturing strategies based on continuous processing that is integrated with online monitoring tools, or process analytical technology (PAT), coupled with efficient automatic feedback control systems. Closed-loop feedback control system enables the transition toward a more desirable quality by design-based (QbD), rather than quality by testing-based, manufacturing of the next generation of pharmaceutical products. This approach utilizes an optimal consumption of time, space, and resources, while satisfying the high regulatory expectations, flexible market demands, operational complexities, and economic limitations. Due to globalization of the pharmaceutical market, the effective patent life and overall profitability of newly discovered drugs have also decreased considerably, forcing pharmaceutical companies to minimize the drug development time and maximize the throughput. Likewise, ferocious price competition after the loss of exclusivity makes reductions in the cost of goods sold, a primary target [1]. However, due to the different levels of complexities involved (e.g., solid handling, irregular flow, complex granulation mechanisms) and the unavailability of suitable process models, control hardware platforms, and real-time sensors, the design and implementation of an efficient control system to enable QbD-based manufacturing in the manufacturing of solid dosage forms is still an open area of research.

Granulation is a size enlargement process that is crucial to pharmaceutical manufacturing processes. Tablet manufacturing via wet granulation is the most common processing route used in the pharmaceutical industry. Other modes of tablet manufacturing are direct compaction, typically the simplest route, and dry granulation, which is especially suitable for hygroscopic APIs. Granulation is a critical unit operation that provides enhanced flowability characteristics of the powder blends and largely affects the end product quality (e.g., tablet hardness and dissolution). Therefore, granulation is particularly important from a control perspective. Due to the lack of a mechanistic understanding of particulate processes, granulation is currently operated inefficiently in practice with high recycle ratios [2]. The proper regulation and control of such particulate processes in the pharmaceutical industry is of much importance given the imposition of tight quality criteria by the regulatory authorities [3, 4].

The four main types of continuous wet granulation processes are high shear, fluidized bed, drum, and twin-screw granulation (TSG). Of these four categories, twin-screw granulation (considered in this study) shows particular potential for pharmaceutical applications [5, 6]. TSG is a novel unit operation particularly suitable for continuous granulation typically used in continuous tablet manufacturing process. Some of the advantages of TSG include design flexibility, short residence time, ability to handle small capacities, and better ability to mix ingredients. In TSG, powder particles are passed through a twin-screw extruder, and a liquid binder is continuously sprayed onto the powder to promote aggregation. Unlike high-shear and fluidized bed granulation, TSG processes operate at lower capacities that are typically required in pharmaceutical manufacturing. Additionally, the configuration of the screw elements influences the liquid distribution, degree of mixing, and breakage rates. The screw configuration offers an additional design parameter to optimize the granulation process.

To enable the implementation of a monitoring and control system for a continuous tablet manufacturing process via wet granulation, extensive research has been performed to understand the process dynamics. Model-based dynamic flowsheet simulations have been used as a design tool prior to implementation within the pilot-plant manufacturing facility at the Engineering Research Center for Structured Organic Particulate Systems (ERC-SOPS). The model-based virtual experimentation approach helps to optimize resources by reducing the number of real experiments needed for the design and optimization of a continuous process and the implementation of an efficient control system.

In the last few years, very few attempts have been made towards the control of a tablet manufacturing process. Singh et al. have suggested a monitoring and control system for a batch tablet manufacturing process [7]. Hsu et al. have suggested a control system for a roller compactor, an important unit operation used for a dry granulated continuous tablet manufacturing process [8, 9]. Ramachandran and Chaudhury have proposed a control system for a continuous drum granulation process [10]. A detailed review on the control of a fluid bed granulation process has been performed by Burggraeve et al. [11], and discussion has been provided by Bardin et al. on the control aspects for efficient operation of a high shear

mixer [12]. Sanders et al. have performed extensive control studies using proportional integral derivative (PID) and model predictive control (MPC) methods on an experimentally validated fluidized bed granulation model [13]. An MPC approach has been employed for a wet drum granulation process by many researchers [14–16]. Ramachandran et al. have designed a regulatory control system for a continuous direct compaction process with emphasis on blending and tableting process [17]. Singh et al. have developed an advanced MPC system for direct compaction continuous tablet manufacturing process and highlighted the implementation of the control system [18]. Singh et al. have designed a control system for a roller compaction route of the continuous tablet manufacturing process [19]. However, no attempt has been made to design a control system for an integrated continuous tablet manufacturing process via wet granulation [20].

In this study, an efficient control system for an integrated continuous pharmaceutical tablet manufacturing process via wet granulation has been designed. The designed control system has been implemented into a mathematical model simulated in gPROMS to evaluate its performance. Set point tracking and the ability to reject disturbances of the designed control system have been analyzed. The systematic application of the control system enables the industrial practitioners to achieve a predefined end product quality consistently.

In the next section, a continuous tablet manufacturing process via wet granulation and corresponding process model is described. In "Design of the Control System for Continuous Tablet Manufacturing Process via Wet Granulation," the control system design for this process is presented. The performance of the control system is evaluated in "Results and Discussion."

Continuous Tablet Manufacturing Process via Wet Granulation

Process Description

The continuous tablet manufacturing process via wet granulation is shown in Fig. 1. The process diagram conceptually represents a pilot plant situated at Rutgers University as a part of the ERC-SOPS. Some details of the pilot plant have been previously reported [21], and the open-loop operation has been extensively studied [3, 4, 22–24]. As shown in Fig. 1, there are three gravimetric feeders to provide the necessary lubricant, API, and excipient. The feeders contain a hopper that can hold a certain amount of material and a rotating screw to change the flow rate. These feeds are then supplied to a blender to generate a homogeneous mixer. Before the blending process, a milling step can be also used for delumping purposes if necessary. The outlet from the blender is fed to a

hopper to maintain a certain amount of the material holdup to flow into the wet granulator.

A TSG is used to granulate the primary powder. A photograph of the considered TSG is shown in Fig. 1. In this figure, the conveying elements and the kneading blocks have been highlighted. The continuous TSG has three different zones, as shown in Fig. 1. The feed powder is introduced in premixing zone where the API, excipient, and lubricant are well mixed. The liquid binder is added to the granulator in the next axial zone. Finally, in the wet massing zone, the granules are formed. The granules obtained from the TSG are then sent to a dryer to achieve the desired moisture level. The dry granules can be passed through a milling machine (e.g., hammer mill) to break the lumps or over-sized granules formed during the granulation process. The granules obtained from the milling machine are then sent to a hopper. From the hopper, the powder granules are fed to a tablet press through a feed frame. Final compacted tablets are then obtained from the tablet press. Among them, some tablets are collected for dissolution testing. This process flowsheet has been implemented using the simulation software gPROMS (Process Systems Enterprise, http://www.psenterprise.com/). The methodology to develop an integrated process flowsheet has been described by Boukouvala et al. [3].

The control of processes involving solid handling (such as in tablet manufacturing) is more challenging than that of fluid-based processes. Solid substances do not flow smoothly, and process delays are often involved due to sensor placement and the slower flow behavior of powder materials. In addition, the process variables are highly interactive, which can affect the overall closed-loop control system performance. The different phenomena involved in the tablet manufacturing process are also poorly understood, making the selection of control variables and pairing of control variables with the optimal actuator a difficult task. Many unit operations (e.g., granulation) involve complex process mechanisms that exhibit non-linear process dynamics and are difficult to control. For example, the mechanisms influencing the granulation process can be summarized as (1) wetting and nucleation, (2) aggregation and consolidation, (3) breakage and attrition, and (4) layering. The various sub-processes involved in granulation have strong interactions with each other. The agglomeration of fine powder occurs due to the presence of surface liquid on the particles resulting from the inherent wetness of the particles or the addition of external liquid. Consolidation also aids in the aggregation process as it leads to the liquid being squeezed out to the surface, which then enhances agglomeration. Breakage and attrition lead to a reduction in the particle size as larger particles form smaller fragments. Layering leads to a reduction in the fines and a net increase in the particle size due to the deposition of fines on coarse particles. The various input operating parameters affecting granulation have been identified as the impeller speed and the flow rate of the binder [25].

Fig. 1 Continuous tablet manufacturing process via wet granulation with snap shot of important process equipment
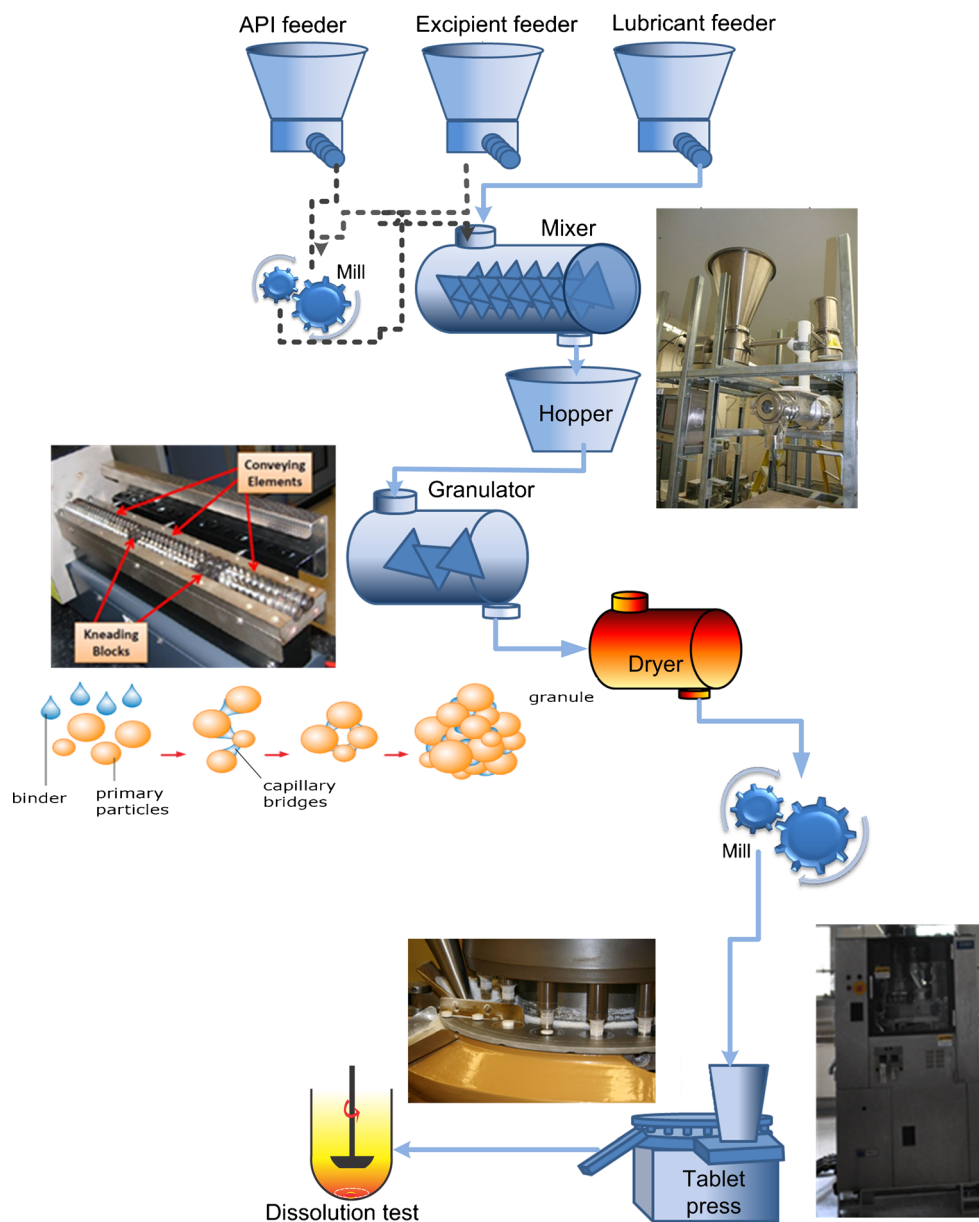
These have been observed to significantly affect the granule properties and hence are vital from a process control perspective.

Process Models

In order to perform virtual experimentation, extensive research has been undertaken to develop the flowsheet model for the continuous tablet manufacturing process via wet granulation. The detailed developments of these models are reported elsewhere and summarized here. The mathematical model for powder blending, an important but complex unit operation, has been previously developed by Sen et al. [26–28]. A population balance-based model for the granulation process has been presented in Barrasso and Ramachandran and Barrasso et al. [29, 30]. A model for the tablet compression process is previously reported in Singh et al. [7]. This model is based on the Kawakita and Ludde powder compression model [31]. The dissolution model has been adapted from Kimber et al. [32]. The models for the different unit operations have been created within a gPROMS library to facilitate integrated flowsheet modeling. The approach to forming the integrated process flowsheet using individual unit operation models has been previously demonstrated [3, 20]. Controller models have been selected from the in-built Process Model Library of gPROMS. The detailed models used for design of a control system for the continuous tablet manufacturing process via wet granulation are presented in the "Appendix."

Design of the Control System for Continuous Tablet Manufacturing Process via Wet Granulation

A process control system for the tablet manufacturing process via wet granulation has been designed using the methodology reported in Singh et al. [19]. The final product specifications include tablet weight, tablet hardness, and tablet dissolution. The unit operations are shown in Fig. 1. API, excipient, and lubricant are important feeds to the process.

Critical Process Controlled Variables and Control Options

The critical control variables were selected based on experimentation and model-based analysis. The variables that are not self-regulating, affect product quality, must be kept within equipment and operating constraints, or seriously interact with other controlled variables should be controlled [33]. The critical process points and corresponding controlled variables are listed in Table 1 [17, 19]. A methodology to identify the critical controlled variables was previously developed [34] and implemented into a software [7]. The critical process parameters and critical quality attributes of this process as desired by regulatory authorities (e.g., FDA) are also indicated in the table. For one control variable, there may be many actuator candidates. Therefore, all actuator candidates for each control variable are also listed in Table 1. The best actuator for each control variable is selected in the subsequent step. Depending on the process delay, a control variable can be controlled by a single-loop controller or a cascade controller. For the single-loop controller, one measurement sensor and one controller (e.g., PID) are required, while for the cascade controller, two measurement sensors and two controllers (master

and slave) are needed. Because of these needs, the cascade controllers are more expensive. In cascade mode, the master controller generates a set point for the slave controller. The cascade controller can improve the control system performance over a single-loop controller in many instances. For example, when a large time delay is involved or when disturbances affect a measurable intermediate that directly affects the controlled variable, the gain of the secondary process, including the actuator, is nonlinear and more difficult to tune. The possible control loop options (single loop/cascade) are also given in Table 1.

Controller Configuration

The identification of a suitable manipulated variable (actuator) for each control variable is important for satisfactory control loop performance. In general, the actuator should have a large, rapid, and direct effect on the control variable with minimal process delay time. The relative gain array (RGA) method [35] or dynamic sensitivity analysis method [19] can be used to identify suitable actuators. The RGA method is based on the steady state analysis and does not take into account the dynamic behavior of the process, while the dynamic sensitivity analysis method takes into account the effect of actuator candidates during the duration of process operation. In a dynamic sensitivity analysis method, the actuator candidates are perturbed (e.g., −3 to +3 %), and the absolute percent change in controlled variable ($100 \left| \frac{Y_0^j(t) - Y_i^j(t)}{Y_0^j(t)} \right|$) is analyzed. The actuator that results in the highest change in control variable is selected as the final actuator.

Table 1 Controller configuration for controlled variables and their actuators

Critical process points	Controlled variables	Actuator candidates	Controller loop
Blender	Total flow rate at blender outlet (CPP)	Rotation speed of powder feeders, rotation speed of blender	Single/cascade
	API composition (CQA)	Ratio set point, rotation speed of blender	Single/cascade
	Ratio (CQA)	Rotation speed of powder feeders	Single
Granulator	Average granule size (CQA)	Binder flow rate, screw rotational speed	Single/cascade
	Granule size distribution ($\sqrt{d84/d16}$) (CQA)	Binder flow rate, screw rotational speed	Single/cascade
	Bulk density (CQA)	Binder flow rate, screw rotational speed	Single/cascade
Dryer	Moisture content (CPP)	Heat inlet	Single/cascade
Tablet press	Tablet weight (CQA)	Feed volume, pre-compression pressure[a], main compression pressure[a]	Single/cascade
	Tablet hardness (CQA)	Punch displacement, pre-compression pressure[a], main compression pressure[a]	Single/cascade
	Tablet thickness (CQA)	Punch displacement, pre-compression pressure[a], main compression pressure[a]	Single/cascade
	Tablet dissolution (CQA)	Punch displacement, pre-compression pressure[a], main compression pressure[a]	Single/cascade

CPP critical process parameter, *CQA* critical quality attribute

[a] Intermediate actuator candidates

The granulation operation (using TSG) is presented as a demonstrative example for the selection of an actuator. There are three control variables (average granule size, granule size distribution, and bulk density) and two actuator candidates (binder addition rate and screw rotational speed). This system is an example of a non-square system where the number of control variables is greater than the number of available actuators. Among these three control variables, only two variables can be controlled independently. Therefore, the first two control variables need to be selected and paired with the suitable actuator. The dynamic sensitivity analysis method is used to identify the most sensitive actuator for each control variable. Since at any time instance, the granule size distribution is not a constant numeric value, it cannot be controlled as such. In order to quantify the granule size distribution for control purposes, a descriptive parameter of the spread, $\sqrt{d84/d16}$, is considered as the control variable. Controlling this variable ensures that the desired granule size distribution is achieved.

The sensitivity of binder flow rate and screw rotational speed on average granule size is shown in Fig. 2. Figure 2a shows the dynamic sensitivity response while Fig. 2b shows the sensitivity response at steady state. The step changes from 3 to −3 % with step size one has been made in actuator candidates and the resulting percent change in control variable (absolute value) has been recorded. As shown in Fig. 2a, the average granule size is much more sensitive to the binder flow rate than it is to the screw rotational speed throughout the operation. Figure 2b shows more clearly that at steady state, binder flow rate is more sensitive than screw rotational speed. Therefore, the binder flow rate can be selected as the actuator for the control of average granule size. Similarly, the sensitivity analysis of the binder flow rate and screw rotational speed on granule size distribution and bulk density has been performed. In comparison to the screw rotational speed, the granule size distribution is found to be much more sensitive to the binder flow rate, and therefore, the binder flow rate can be selected as the final actuator (result is not shown). The bulk density is more sensitive to the screw rotational speed than it is to the binder flow rate, so the screw rotational speed is the suitable actuator for the control of bulk density. Since the average granule size and the granule size distribution have the same actuator, only one of them can be controlled independently. In order to identify whether the granule size or the granule size distribution should be controlled, the sensitivity of these variables to the binder flow rate is compared. The average granule size is more sensitive to the binder flow rate, so the average granule size can be controlled using the binder flow rate as the actuator while ensuring that the granule size distribution also follows the desired trajectory. Similarly, the actuator for the other controlled variables has been identified as given in Table 2.

Table 2 also shows whether the single-loop controller is sufficient or a cascade controller is desired corresponding to each control variable. Based on the controlled variable and corresponding actuator relationship, it is also identified whether direct action (increasing the actuator increases the control variable) or reverse action (increasing the actuator decreases the control variable) is needed. This information is useful to calculate the deviation and to implement the control action. In the case of direct action, the error (deviation) is calculated as $y-y_{set}$, while in case of reverse action the deviation is calculated as $-(y-y_{set})$.

PAT Techniques and Tools

Within the ERC-SOPS, measurement techniques and tools for the real-time measurement of the different variables involved in the continuous tablet manufacturing pilot plant are being evaluated. These techniques are combined with the proposed control system to integrate into the pilot plant, which is a subject of research and development within the center. Some of the monitoring techniques are reported in the scientific literatures [7, 23, 36–41]. API composition and relative standard deviation (RSD) are measured by NIR sensor (JDSU micro NIR, Bruker Matrix). Powder flow rate can be measured by load cell. In tablet press, compression forces are measured by strain gauge; tablet weight and hardness are measured by checkmaster (Fette) while a soft sensor can be employed for dissolution measurement. Soft sensors are inferential estimators, drawing conclusions from process observations when hardware sensors are unavailable or unsuitable [42]. Soft sensing toolbox is available in commercially available control platform (DeltaV (Emersion)). Efforts are also being made to develop the technique for real-time monitoring of dissolution [43].

On-line monitoring for a continuous twin-screw granulation process has been demonstrated in El Hagrasy et al. [44]. The product stream is fed through a chute and illuminated with an LED. An Eyecon high-speed camera was positioned in line with the stream, capturing images of the full particle size range. Images were taken at 2–3 s intervals. The images were analyzed in real time to identify a set of ellipses, and the size estimate for each moment of the distribution was computed based on the current and most recent images based on a 30-s moving window. These results were consistent with sieve measurements. The particle count was also calculated. This technique demonstrated sensitivity to process perturbations. The particle count, $d10$, $d50$, and $d90$ values showed responses as a step change was applied to the liquid-to-solid ratio from 0.2 to 0.3. The $d10$ value and particle count had the most stable responses with the least variability, demonstrating their potential for process monitoring and control.

One of the most powerful PAT techniques to monitor the pharmaceutical tablet manufacturing process is NIR.

Fig. 2 Selection of actuator for average granule diameter control. **a** Dynamic sensitivity analysis, **b** response at steady state
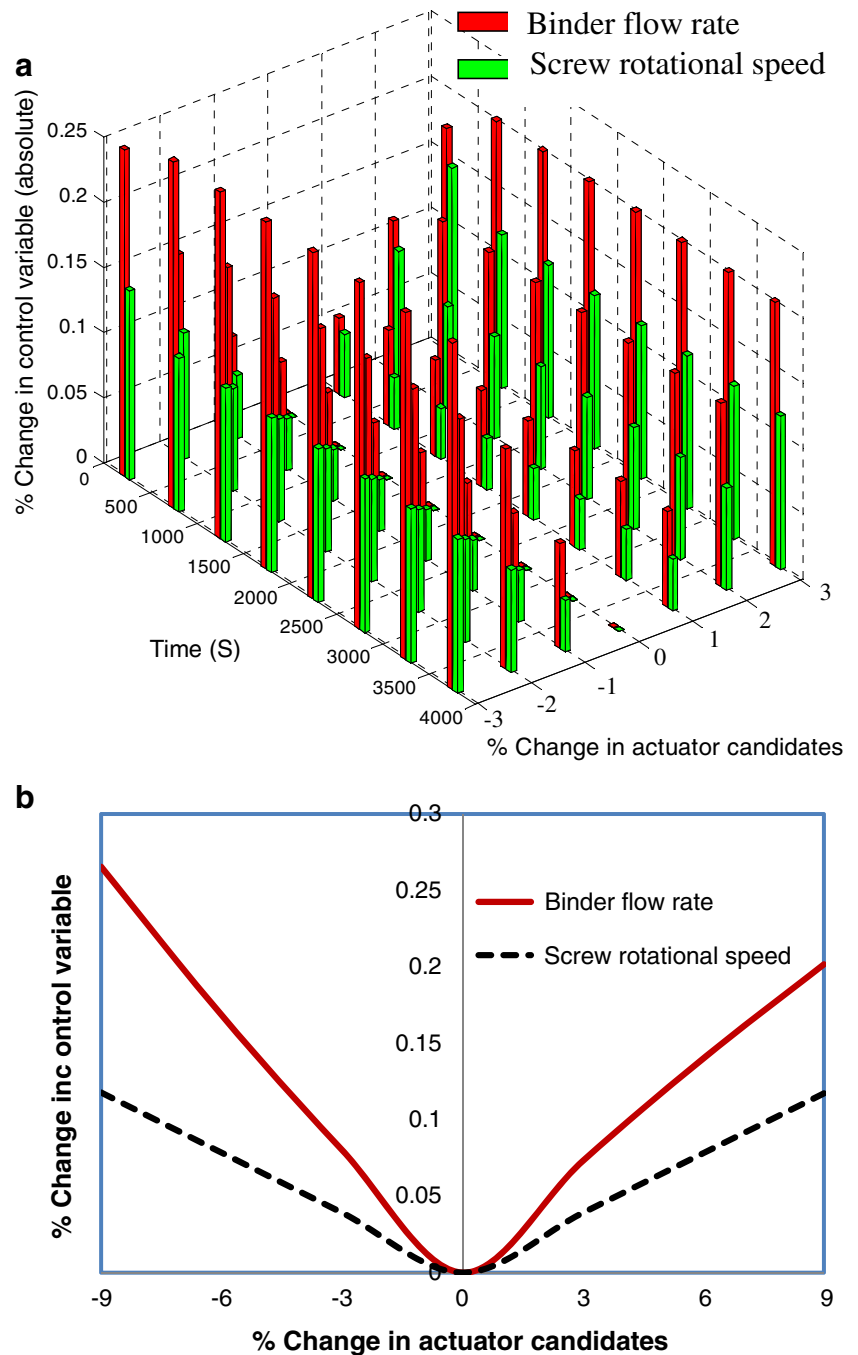
However, its application for feedback control is still in early research stages. The NIR sensor has been integrated with the plant and the control platform (DeltaV) through the OPC (object linked and embedding for process control) communication protocol as described here, using the powder blending process as the demonstrative example. OPC is the standard system for the real-time plant data communication between control devices from different manufactures [42]. A chute has been used to interface the NIR (JDSU) with the continuous blender. The spectrum collected by NIR is then sent to a

computer (DeltaV application station PC) in which software for prediction (Unscrambler X, prediction engine, process pulse) and for communication (MATLAB OPC) are installed. Unscrambler X Process Pulse uses prediction engine and the prediction model (developed in Unscrambler X) to generate the API composition signal. The NIR prediction model is uploaded into process pulse, and the spectrum obtained by JDSU NIR is stored. The output file containing the API composition is linked with the MATLAB OPC tool which sends the data to the DeltaV system.

Table 2 Controller configuration

Critical process points	Controlled variables	Intermediate actuator	Actuator	Controller loop	Control action
Blender	Total flow rate at blender outlet (CPA) (y_1)	Input for ratio controller (F_{T_set})	Rotation speed of feeders (u_{11}, u_{12}, u_{13})	Cascade controller	Direct
	API composition (CQA) (y_2)	Set point for ratio controller	Rotation speed of feeders (u_{11}, u_{12}, u_{13})	Single-loop controller	Direct
	Ratio (CQA) (y_3)	–	Rotation speed of feeders (u_{11}, u_{12}, u_{13})	Ratio controller	–
Granulator	Average granule size (CQA) (y_4)	–	Binder flow rate (u_4)	Single-loop controller	Direct
	Bulk density (CQA) (y_5)	–	Screw rotational speed (u_5)	Single-loop controller	Reverse
Dryer	Moisture content (CPA) (y_6)	–	Heat inlet (u_6)	Single-loop controller	Reverse
Tablet press	Tablet weight (CQA) (y_{71})	Pre-compression pressure (y_{72})	Feed volume (u_7)	Cascade controller	Direct
	Tablet dissolution (CQA) (y_{81})	Hardness (CQA) (y_{82}), main compression pressure (y_{83})	Punch displacement (u_8)	Three controllers	Reverse

CQA critical quality attribute, *y* control variable, *u* actuator

Controller Parameters Tuning and Controller Inputs

As given in Table 2, there are three cascades, four single-loops, one cascade with three controllers and one ratio controller involved in the process. Therefore, a total of 13 PI(D) controllers are required, and a maximum of 39 controller parameters need to be tuned. There are several methods and rules for PID controller parameter tuning. Among them, the continuous cycling-based heuristic method proposed by Ziegler and Nichols [45] and optimization-based methods (integral of time absolute error (ITAE), IAE, ISE) are widely used in the process industries [33]. In this work, the Ziegler and Nichols method has been employed first to get initial values for tuning the controller parameters. Then the optimization based method (ITAE) has been used to fine tune these parameters. The flowsheet model of continuous tablet manufacturing process via wet granulation simulated in gPROMS has been used to perform the optimization.

The anti-windup reset algorithm [46], which ensures that the controller output lies within the specified upper and lower bounds, has been included. Because of anti-windup, if the bounds are violated, the time derivative of the integral error is set to zero, and the controller output is clipped to the bounds. Once the controller output is back in the range of the bounds, the integral error will change according to the current error.

Similarly, to change the value of the derivative part with certain factor, a term called the rate limit has been introduced. If the value of the rate limit is one, the calculated derivative term and the applied derivative term are the same, while a rate limit value of less than one means the applied derivative term is more than the calculated value. A rate limit value greater than 1 means the applied derivative term is less than the calculated value. To avoid obtaining undesired controller outputs, minimum and maximum limits of the controller output have been introduced. The anti-windup algorithm will keep the controller output within the specified limit. The minimum

and maximum limits of the controller input have also been defined to improve the controller performance. However, the controller inputs can violate the specified limits. Scaling factors for controller input, output, and set point have been introduced to improve the controller performance.

Other than tuning the controller parameters, there are additional control parameters (minimum input, maximum input, minimum output, maximum output, bias, rate limit) that should be specified appropriately to achieve better controller performance. The tuned control parameters, together with these specifications, are given in Table 3.

Proposed Control System

Based on the above analysis, a control system for the continuous tablet manufacturing process via wet granulation is proposed. The control system is implemented using a flowsheet model of the process (simulated in gPROMS) to evaluate its performance. The designed control system is shown in Fig. 3. The control variables, actuators, and input/output signal from each PID controller are also shown in Fig. 3.

Note that depending on the type of process equipments used, available sensors, and process configuration, the proposed control system may need to be adapted for a specific case. In the blending process, blend composition at blender outlet and total flow rate from blender needs to be controlled. The set point of total flow rate could come from another master controller (not included here), such as a controller specially designed to accommodate the variations in turret speed. However, the change in the total flow rate should be small so that it does not violate the blender operational constraints (required powder holdup, required residence time). To control the blend uniformity, different options could be explored, including for example implementing a gate valve in the blender that can be adjusted in real time to increase/decrease holdup and, therefore, blade passes. This approach

Table 3 Controller parameters and other controller specifications

Control loop	Controller	Gain (K_C)	Reset time (K_I)	Rate (K_D)	Minimum input	Maximum input	Minimum output	Max output	Bias	Rate limit	Control action
	$C_{1,2}$	0.01	1	0.5	0	1	0.00001	1	0	1	Direct
Flow rate	$C_{2,1}$	0.8	0.001	10	15	25	0.01	10	0	1	Direct
	$C_{2,2}$	2	0.0005	0.5	9	11	0.6	0.8	0	1	Direct
API composition	C_3	0.02	0.01	0.01	0	1	0.001	6	0	1	Reverse
Ratio	C_4	–	–	–	0	1	0	1	0	–	–
Average granule size	C_5	0.01	100	1	205	215	0.001	0.6	0	1	Direct
Granules bulk density	C_6	100	10	1	1,450	1,470	2	3,200	0	1	Reverse
Moisture content	C_7	1	10	1	0	1,000	0	1	0	1	Direct
Weight	$C_{8,1}$	1	10	0	2E−4	4E−4	5	20	0	1	Direct
	$C_{8,2}$	1	10	0	14	16	2E−6	3E−6	0	1	Direct
Dissolution	$C_{9,1}$	10	0.01	0	0.89	0.95	50	160	0	1	Reverse
	$C_{9,2}$	10	0.01	1	100	140	0.001	30	0	1	Direct
	$C_{9,3}$	5	10	10	0.001	0.02	1E−7	2.3E−3	0	1	Direct

can be used to change the blender speed while keeping the blender holdup constant.

A ratio controller calculates the set points of the API, excipient, and lubricant flow rates. Then, the built-in slave controller in each feeder tracks these set points. The set points for the total flow rate and ratio are the two inputs for the ratio controller, which comes from master controller.

In the granulation process, the average granule size is controlled by manipulating the binder flow rate through a single PID controller. It can be seen in Fig. 3 that the granule size is the input to the PID, while the binder flow rate is the output. Similarly, the bulk density is controlled by manipulating the screw rotational speed through a single PID controller.

For the dryer, the moisture content is controlled by manipulating the heat inlet. Milling is only used in this process for delumping purposes, so no controller is needed for the milling process.

For the tablet pressing process, the tablet weight is controlled using a cascade control scheme. As shown in Fig. 3, the measured weight is the input for the master controller that generates the set point for the slave controller. The slave controller controls the pre-compression pressure by manipulating the powder feed. Three PIDs are used in series to demonstrate the concept of dissolution control. The dissolution can be monitored through the soft sensor that is the input for master controller. This master controller then generates the hardness set point for slave controller. This hardness is controlled through a cascade control scheme. If so desired, the hardness set point can be directly provided by the user and the dissolution controller can be ignored. For hardness/dissolution control, the main compression pressure is used as the intermediate actuator, while the punch displacement is used as the final actuator. In this way, the pre-compression pressure is utilized to

control the tablet weight, and the main compression pressure is utilized to control the tablet hardness/dissolution.

Utilizing the pre-compression pressure for feedback control is, however, a challenging task since its magnitude is normally very small. These two cascade control loops can be simplified if required by removing one slave controller that required pre-compression force. The tablet weight and hardness can be controlled through a cascade control arrangement using two master loops and one slave loop. Master loops are used to control the weight and hardness and provide the set point for the slave controller, which controls the main compression pressure by manipulating the fill depth. In the simplified scenario, the tablet weight is measured and controlled more frequently, while the tablet hardness is measured and controlled less frequently and shares a common slave controller, meaning that only one master controller is activated at a time. Note that the hardness control loop is activated only when the measured hardness deviates by a certain percentage (e.g., 5 % of set point) from the desired set point. The performance of the implemented control system has been evaluated in "Results and Discussion."

Results and Discussion

Prior to the implementation of the control system into the continuous tablet manufacturing pilot plant via wet granulation, the performance of the designed control system is evaluated as described in this section. The model-based performance evaluation of the control system reduces the time and resources needed for the implementation of the control system into the pilot plant and increases the chance of success during implementation. In this section, the ability of the control system to track the set point and reject the disturbances is
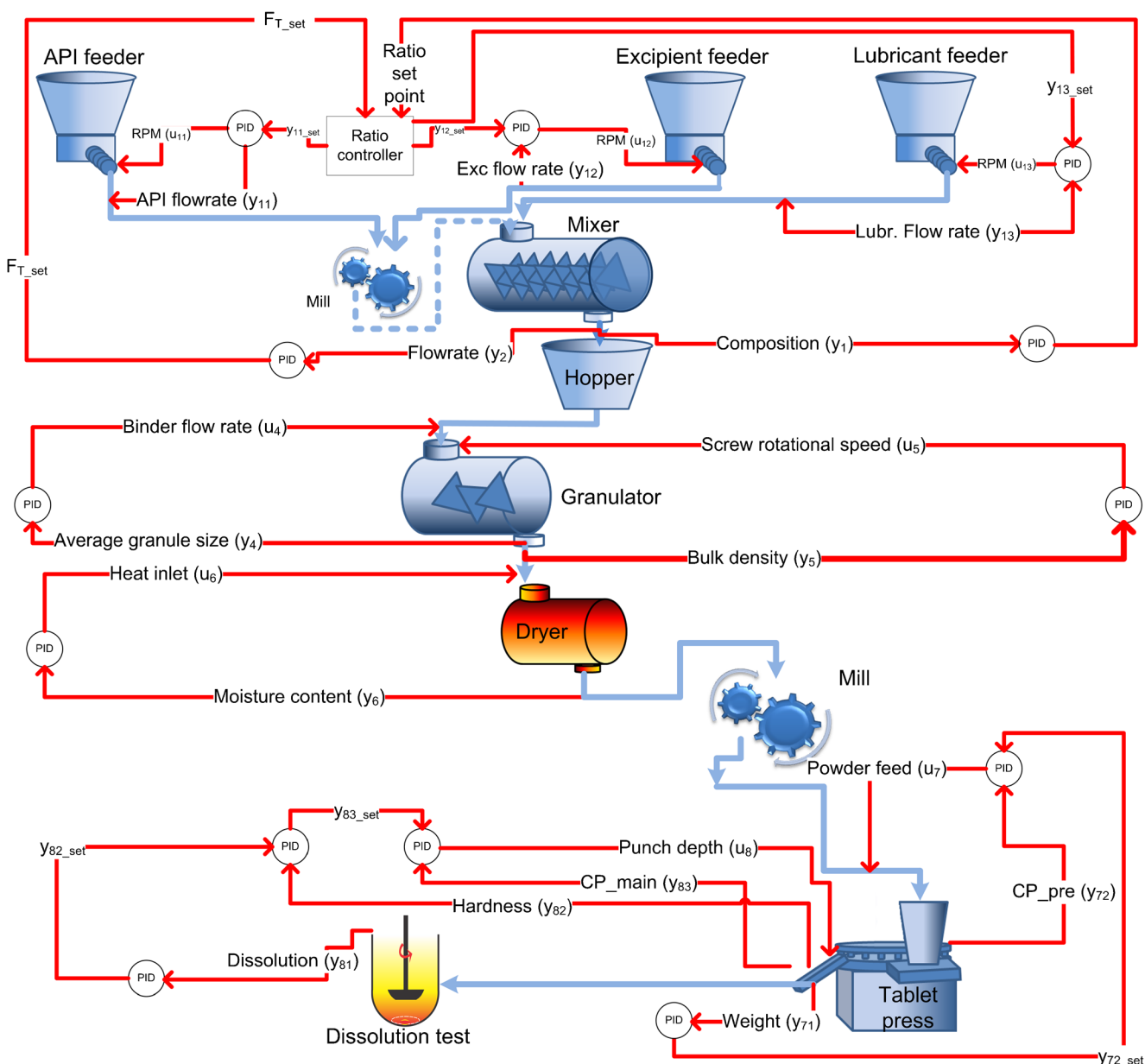
Fig. 3 Control system for the continuous tablet manufacturing process as implemented in a flowsheet model

evaluated. For set point tracking, the step changes in the set point are applied, and the controller is allowed to track those changes. For disturbance rejection, structural disturbances (e.g., sinusoidal) and random disturbances are introduced during closed-loop operation.

The Ability of the Controller to Track the Set Point

More often, the set points of the process variables need to be changed during plant operation. For example, to change the throughput, it is necessary that a controller tracks the set point. The granulation process is considered here as a demonstrative example. A signal delay of 20 s has been introduced that accounts for process and sensing delays. A structural

sinusoidal disturbance with amplitude of 50 μm has been also introduced to accommodate process and sensing disturbances (disturbance=$50 \times \mathrm{Sin}(t)$). The random variability, as well as structural (sinusoidal) variability, has been also added into the quality attributes (particle size, bulk density) of the input materials. The closed-loop response of the granule size controller for set point tracking is shown in Fig. 4. The step changes in the average granule size are introduced, and a single PID controller tracks the set point. The figure shows that the controller is able to track the set point with reasonable accuracy. As desired for a good controller, the rise time and the deviation from the set point are small. The sudden over-shoot at the point of the step change is over a very small time interval and can be accepted. The average granule size is
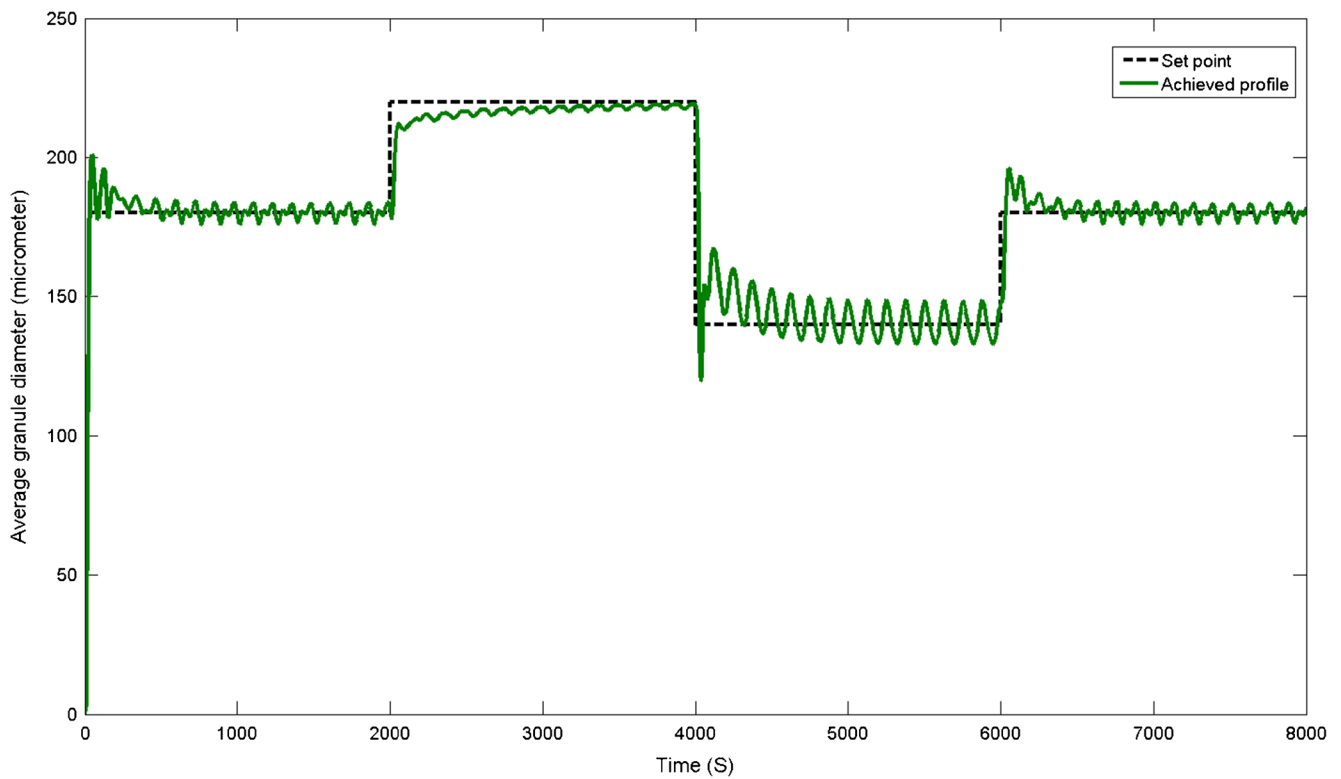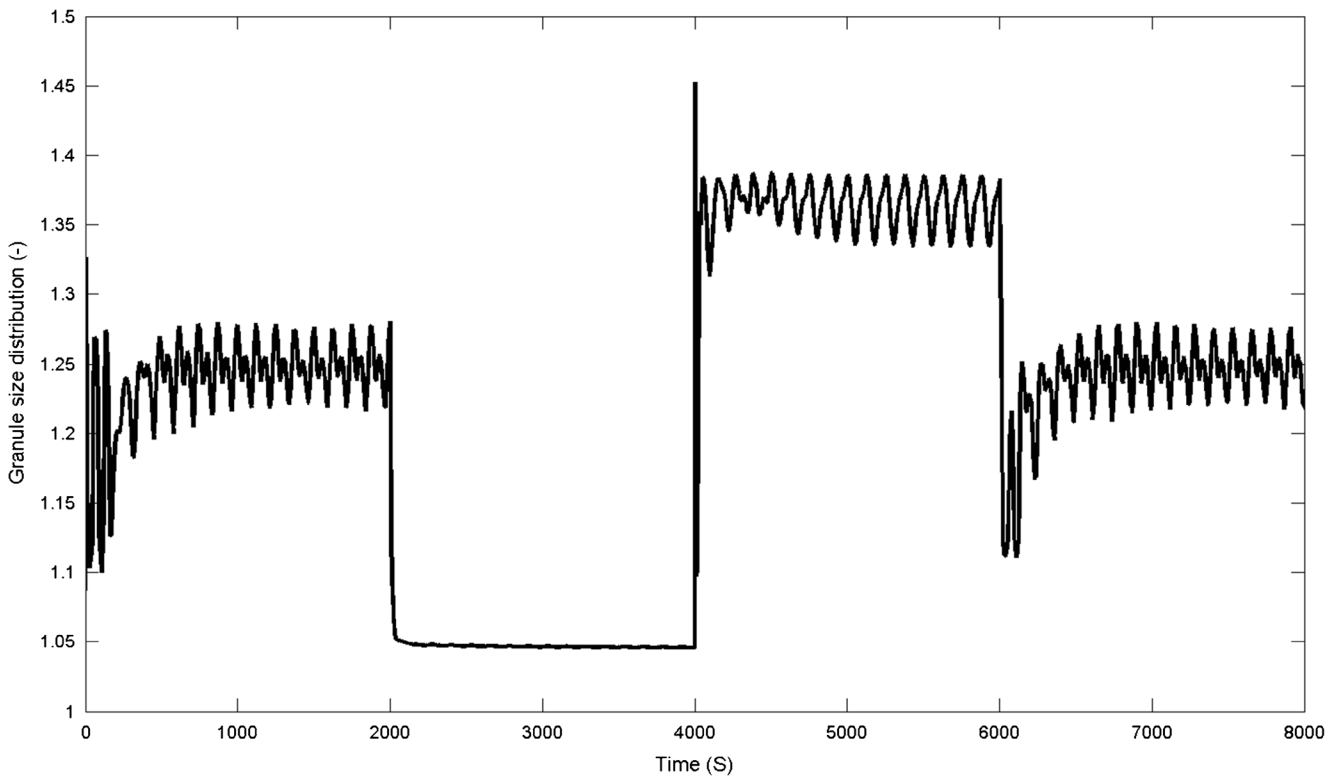
Fig. 4 Closed-loop response of average granule size (set point tracking)

controlled by manipulating the binder flow rate. The disturbances for this control loop come from the powder feed as well as the blending operation. Average granule diameter

control loop (see Fig. 4) and bulk density control loop (see Fig. 5) have high interaction since binder flow rate and screw rotational speed can affect both control variables.
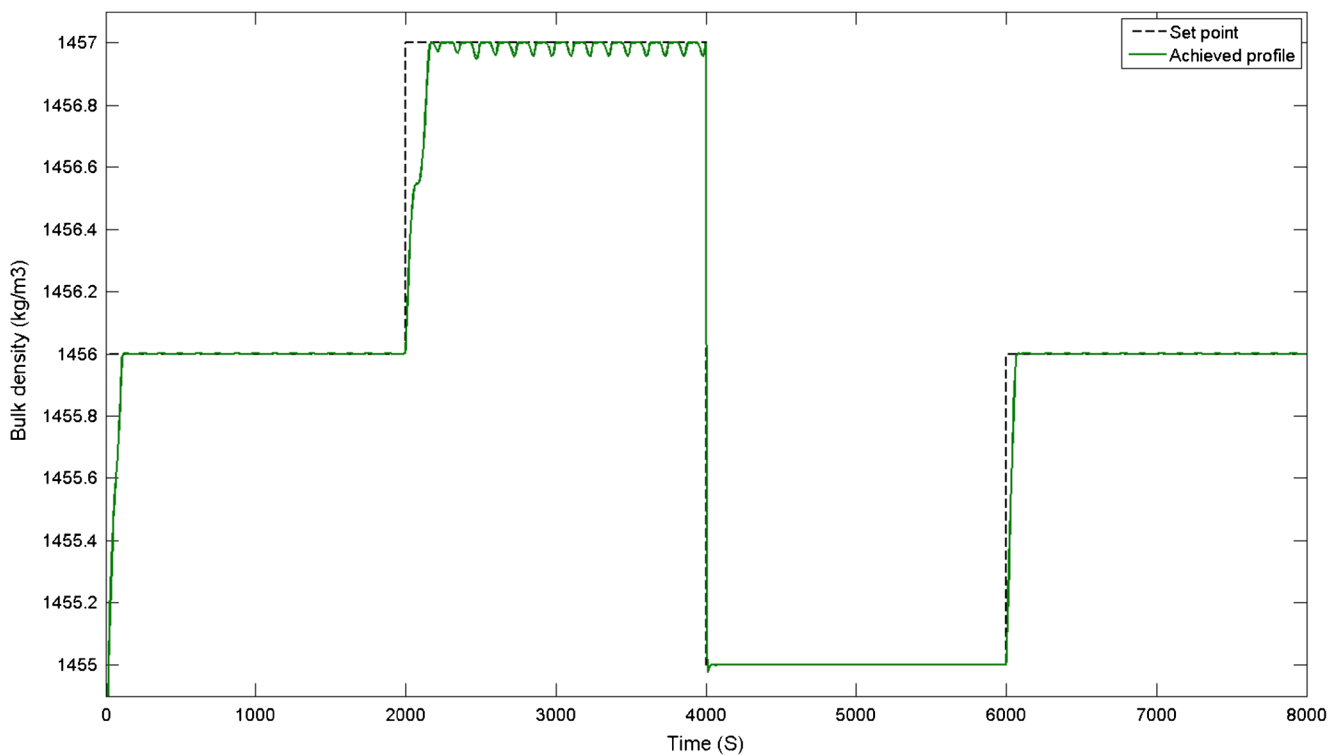
Fig. 5 Closed-loop response of bulk density (set point tracking)

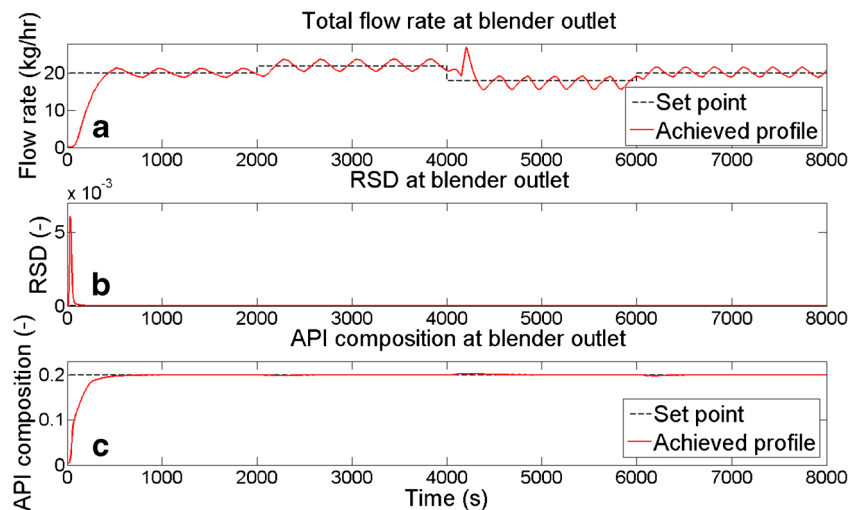**Fig. 6** Response of the granule size distribution

Oscillatory response of average granule diameter from 4,000 to 6,000 s is because of these control-loop interaction. However, the maximum error is within 10 μm which is acceptable. The changes in powder feed properties (e.g., particle size, bulk density) affect the granule size, as well. The ITAE [33] value for closed-loop response is 3.72E7 μm s. The root mean square error (RMSE) is 30.81 μm which is acceptable.

The closed-loop response for bulk density control is shown in Fig. 5. A structural sinusoidal disturbance has been introduced to accommodate process and sensing

disturbances (disturbance=$0.1\sin(t/20)$). The controller is able to track the set point with an acceptable rise time. The bulk density is controlled by manipulating the screw rotational speed. The ITAE [33] value for closed-loop response is 2.53E5 kg/m^3 s. The RMSE is 0.3 kg/m^3 which is acceptable.

The response of the third variable (granule size distribution: $\sqrt{d84/d16}$) in the granulation process is shown in Fig. 6. As shown in the figure, the response of this variable is similar to the closed-loop response of the average granule size. Therefore, it can be concluded that

Fig. 7 Closed-loop response of variables involved in blending operation (set point tracking). **a** Total flow rate from blender outlet, **b** relative standard deviation (*RSD*), **c** API composition

Fig. 8 Closed-loop response of variables involved in tablet press (set point tracking). **a** Tablet weight control, **b** tablet dissolution control, **c** tablet hardness control
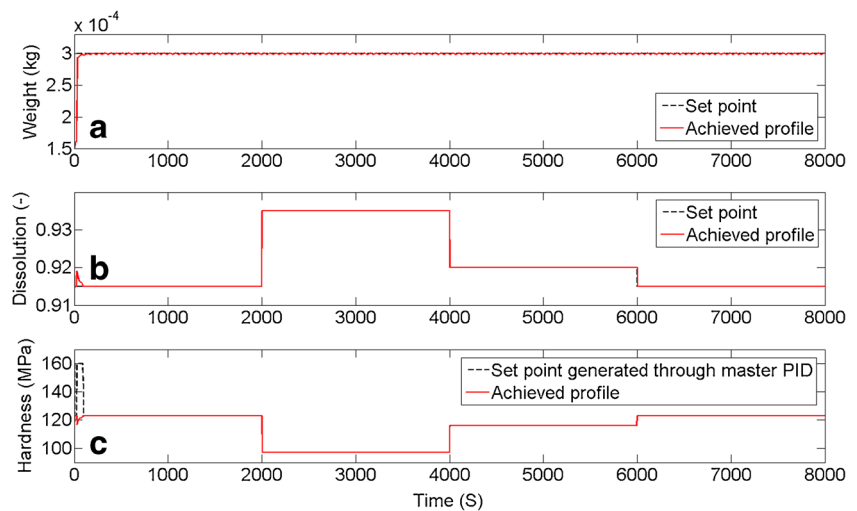
controlling the average granule size assures that the granule size distribution is at the desired value.

Similarly, in the blending operation, the total flow rate at blender outlet and API composition are controlled. The controller performance is shown in Fig. 7. The throughput from blender may need to change while the API composition should be held at constant value. Therefore, a step change has been introduced only in the total flow rate. The closed-loop response of the total flow rate is shown in Fig. 7a. The controller tracks the step change in the set point. Some oscillation in the response of the total flow rate has been observed, which may be because of the larger process delay. Since the solid material does not flow as smooth as liquid, a perfect control is difficult to achieve. A cascade PID controller has been used to control the total flow rate from blender. The outlet of the master controller provides the flow rate set point for ratio controller. Adding a Smith predictor into the existing PID control loop or employing an advanced MPC may improve the performance of the total flow

rate control loop, which is the subject of future investigation. It should be noted that the MPC requires linear/non-linear model identification and an online optimization tool and is more complex to implement in comparison to the PI(D) controller.

The response of the RSD is shown in Fig. 7b. RSD is a measure of the homogeneity of the blend powder, and for a well-mixed powder, it should ideally approach zero. Figure 7c shows the closed-loop response of API composition at the blender outlet. The API composition is controlled at the set point, and the rise time is acceptable. The output of the API composition control loop provides the ratio set point for ratio controller. The ratio controller calculates the flow rate set points for the API, excipient, and lubricant feeders, which are then tracked by slave PID controllers built in each feeder.

The closed-loop responses of the control variables involved in tablet press are shown in Fig. 8. Figure 8a shows the closed-loop response of the tablet weight that is maintained at a

Fig. 9 Closed-loop response of average granule size (disturbance rejection)
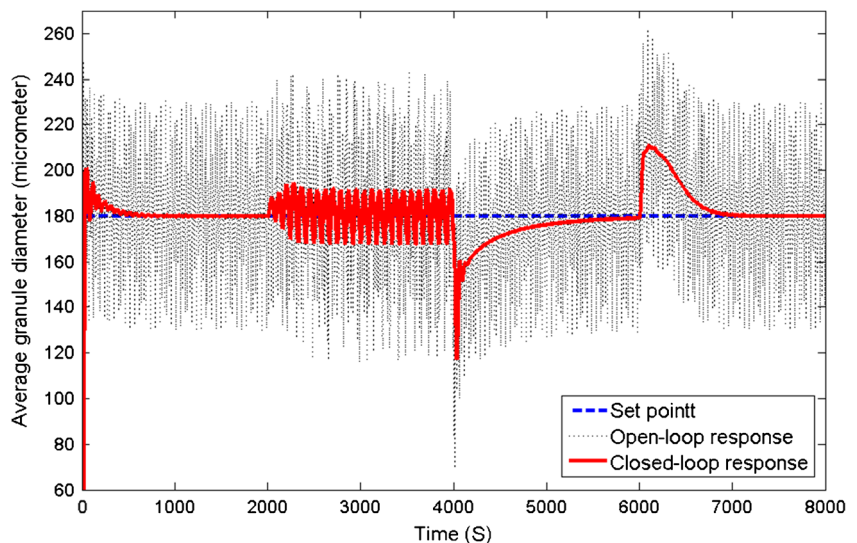
Fig. 10 Closed-loop response of bulk density (disturbance rejection)
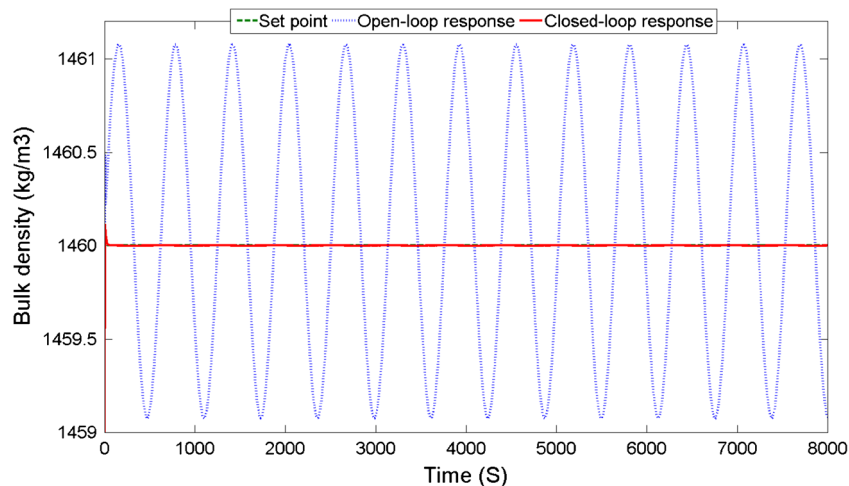
constant set point. The tablet weight is controlled through a cascade control scheme in which the master controller generates the set point of the pre-compression force and the slave controller tracks this set point by manipulating the powder feed. The controller performance is satisfactory. The closed-loop response of dissolution is shown in Fig. 8b. The step change has been introduced in the tablet dissolution to analyze the controller performance. Note that with the available state-of-the-art monitoring techniques, the dissolution cannot be monitored online/inline but can be monitored through a soft sensor [42]. The efforts are also being made to develop the technique for real-time monitoring of dissolution that could be used for control purpose [43]. Three controllers have been used in series to control the dissolution. The first master controller maintains the dissolution at the set point and generates the hardness set point as shown in Fig. 8c. The second controller in series maintains the hardness at the set point (see Fig. 8c) and generates the main compression force set point. The slave controller (third controller in series) maintains the main compression force at the set point and manipulates the punch displacement (final actuator setting). The performance of these controllers is found to be satisfactory.

Disturbance Rejection

In order to analyze the ability of the controller to reject the disturbances, structural sinusoidal disturbances (disturbance $= 50 \sin(t)$) are introduced to the process. The process responses with the open-loop scenario and the closed-loop scenario have been compared. The wet granulation operation is considered here to demonstrate the disturbance rejection ability of the controllers. The response of the average granule diameter is shown in Fig. 9. In the open-loop scenario, the response is oscillatory because of added sinusoidal disturbances. In closed-loop operation, the controller rejects the disturbances and maintains the control variable at the set point. Therefore, it is expected that the designed

controller will be able to reject the unknown disturbances that can occur during the process operation. It should be noted that only one loop at a time is open while other control loops are closed. It can be also seen in Fig. 9 that the response at 2,000, 4,000, and 6,000 s has been deviated from set point because of step changes in bulk density but the controller brings the response back to set point. Because of actuator saturation, the closed-loop response from 2,000 to 4,000 s is oscillatory. However, the magnitude of oscillation is within 15 μm that can be accepted. The ITAE value for closed-loop response is 3.27E7 μm s. The RMSE for closed-loop response is 28.96 μm which is acceptable.

The performance of the controller for bulk density control under disturbances is shown in Fig. 10. The sinusoidal disturbances have been introduced to the bulk density. The closed-loop and open-loop response of the bulk density under disturbances is shown in Fig. 10. In the open-loop scenario, the response is oscillatory because of sinusoidal disturbances, while in closed-loop scenario the controller rejects the disturbances and maintains the bulk density at the set point. The ITAE [33] value for closed-loop response is 1.24E4 kg/m^3 s. The RMSE is 0.21 kg/m^3 which is acceptable. It is expected that the proposed controller can reject any disturbance that occurs during operation. Note that the control loops for the average granule size and bulk densities are interactive and the disturbances introduced in one loop also affect the performance of other loop. Similarly, the disturbance rejection abilities of the other control loops have been analyzed.

Conclusions

A well-designed control system is essential to obtain the consistent, predefined quality of a pharmaceutical product as mandated by regulatory authorities. In this work, we have designed an efficient control system for a continuous tablet

manufacturing process via wet granulation. The considered manufacturing process uses a twin-screw wet granulator as one of the unit operations for producing granules continuously. The proposed control system consists of single-loop and cascade feedback PI(D) controllers, which are simpler and easier to implement into the tablet manufacturing plant. The control system has been implemented in a flowsheet model simulated in gPROMS to analyze its performance. The mathematical model has also been reported. The gPROMS model has been integrated with a DeltaV control platform using gORUN feature of gPROMS and IGEAR software to facilitate the onsite application of the model for controller design (controller parameters tuning) and to provide training on control system. The controller parameters have been tuned using an effective controller parameter tuning strategy involving ITAE methods coupled with optimization routine of gPROMS. State-of-the-art techniques such as an anti-windup algorithm were used to improve the controller performance. The ability of the controllers to track the step changes as well as reject the disturbances was analyzed, and the performance of the control system is found to be satisfactory. Future work includes the implementation of the designed control system in our continuous tablet manufacturing pilot plant through the commercially available hardware (e.g., Delta V) and control interface (e.g., OPC) using the methodology proposed in this work.

Appendix: Continuous Tablet Manufacturing

The mathematical model for the continuous tablet manufacturing process via wet granulation is described in the following section. The model equations have been implemented into a flowsheet model in the gPROMS simulation tool.

Feeder

The feeders are used to supply the API, excipient, and lubricant. The model equations described in Singh et al. has been employed to develop the integrated flowsheet model of the continuous tablet manufacturing process via wet granulation and to implement the control system [18].

Continuous Blender

Process Model

The blending process model that has been integrated with the continuous tablet manufacturing process via wet granulation has been adapted from Sen et al. [26–28]. A population balance modeling framework has been used to model the blending process, and it is assumed that this model is independent of size change. Therefore, the internal coordinates have been dropped from the population balance model. The multi-dimensional population balance model constructed to model blending processes accounts for n solid components and two external coordinates (axial and transverse directions in the blender) and one internal coordinate (size distribution due to segregation). The detail of the blending process model was previously reported [18, 26–28]. The model is summarized as given below.

Population Balance Equation The blending process was modeled using the population balance modeling approach as follows [32]:

$$\frac{\partial F(n, z_1, z_2, r, t)}{\partial t} + \frac{\partial}{\partial z_1}\left[F(n, z_1, z_2, r, t)\frac{dz_1}{dt}\right] + \frac{\partial}{\partial z_2}\left[F(n, z_1, z_2, r, t)\frac{dz_2}{dr}\right] + \frac{\partial}{\partial r}\left[F(n, z_1, z_2, r, t)\frac{dr}{dt}\right]$$
$$= \quad \mathfrak{R}_{\text{formation}}(n, z_1, z_2, r, t) \quad - \quad \mathfrak{R}_{\text{depletion}}(n, z_1, z_2, r, t) \tag{1}$$

where the number density function $F(n, z_1, z_2, r, t)$ represents the total number of moles of particles with property r at position $z = (z1, z2)$ and time t. In addition, z_1 is the spatial coordinate in the axial direction, z_2 is the spatial coordinate in the radial direction, and r is the internal coordinate that depicts particle size. Hence, $\frac{dz_1}{dt}$ and $\frac{dz_2}{dt}$ represent the axial and radial velocity, respectively. It has been assumed that the magnitude of dispersion as compared to convective transport is negligible in powder mixing systems. It has been demonstrated in the works of Portillo et al. [22]. Breakage and agglomeration in blender can be also neglected ($R_{\text{formation}} = R_{\text{depletion}} = 0$).

Below is the spatial discretized form of the PBE for mixing.

$$\frac{\partial F(n, x, y, t)}{\partial t} = \frac{V_{\text{f}}\left[F_{n,x-1,y,t} - F_{n,x,y,t}\right]}{\Delta x} + \frac{V_{\text{b}}\left[F_{n,x+1,y,t} - F_{n,x,y,t}\right]}{\Delta x}$$
$$+ V_{\text{r}}\frac{\left[F_{n,x,y+1,t} + F_{n,x,y-1,t} - 2F_{n,x,y,t}\right]}{\Delta y} + (\text{Inflow} - \text{Outflow})$$

Axial and radial velocity is shown in Figs. 11 and 12, respectively.

In this study, a finite volume scheme has been used where the population distribution has been first discretized into sub-

populations and the population balance is formulated for each of these semi-lumped sub-populations. This is obtained by the integration of the population balance equation over the domain of the sub-populations and re-casting the population into finite volumes. A first-order explicit Euler method has been used for the transient formulation. The rate terms in the PBE are average axial and radial velocities of the particles in each compartment, respectively. These values have been obtained by running a discrete element method (DEM) simulation of the mixer on EDEM™(DEM Solutions). The DEM simulation has been run till the system reaches a steady state and then the velocity values have been extracted. Figures 11 and 12 present the spatial discretization of the mixer and the value of axial and radial velocity terms in each of them.

Algebraic Equations (Explicit) The inlet and outlet powder flow rates of blender are given as follows:

$$\sum_{z_1} m_{in}^i(n = i, z_1, z_2 = 0, t) = m_{in}^i(t) \quad \text{for } i = 1, .., n$$
$$m_{out}^i(t) = \sum_{z_1} m^i(n = i, z_1, z_2 = L, t) \quad \text{for } i = 1, .., n \tag{2}$$

The bulk density is calculated as follows:

$$\rho_{bulk\_out}(t) = \sum_{i}^{n} C(n = i, z_1, z_2 = L, t)\rho_{bulk\_in}^i \tag{3}$$

The mean powder particle size is calculated as follows:

$$d_{50\_out}(t) = \sum_{i}^{n} C(n = i, z_1, z_2 = L, t)d_{50\_in}^i \tag{4}$$

The RSD which represents the homogeneity is calculated as follows:

$$\text{RSD}(t) = \frac{\text{SD}(n ='' \text{API},'' \ z_1, z_2 = L, t)}{\text{mean}(n ='' \text{API},'' \ z_1, z_2 = L, t)} \tag{5}$$

The RSD has been calculated at every axial location by taking samples from all the radial compartments present at that particular axial location. In this model, there are six radial compartments at any axial location. Therefore, the sample size is 6. The RSD reported in this manuscript is calculated at the last axial location (blender outlet). The blending process model is previously validated [28].

-0.0345897 m/s	0.00991314 m/s	0.25754 m/s	0.0882168 m/s	0.300331 m/s
0.0442157 m/s	-0.0128828 m/s	0.321992 m/s	-0.0134739 m/s	0.284365 m/s
0.0398952 m/s	0.0410191 m/s	0.240091 m/s	0.052898 m/s	0.169784 m/s
0.043067 m/s	-0.0585648 m/s	-0.0134552 m/s	0.390047 m/s	-0.216841 m/s
0.04732 m/s	-0.0215878 m/s	-0.153326 m/s	0.248509 m/s	-0.181074 m/s
0.0247718 m/s	0.0597596 m/s	-0.0386316 m/s	0.00408546 m/s	0.0449382 m/s

Fig. 11 Axial velocity

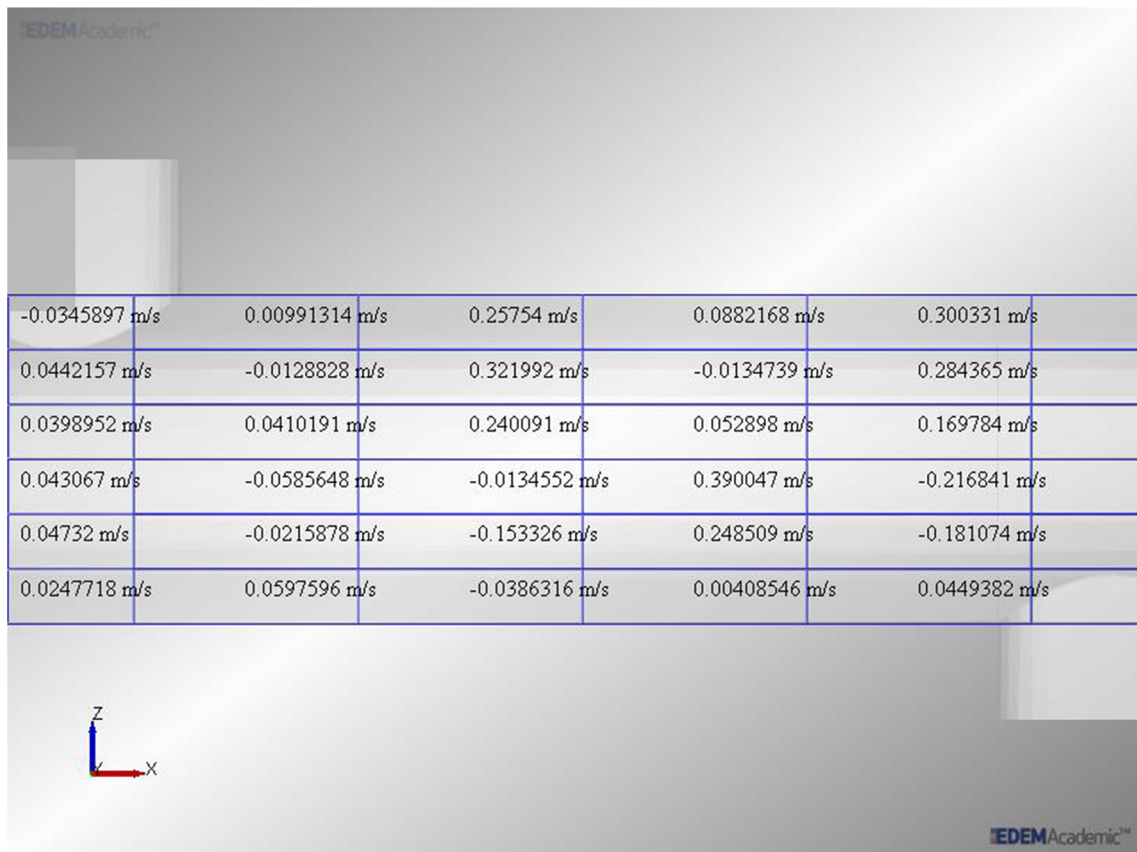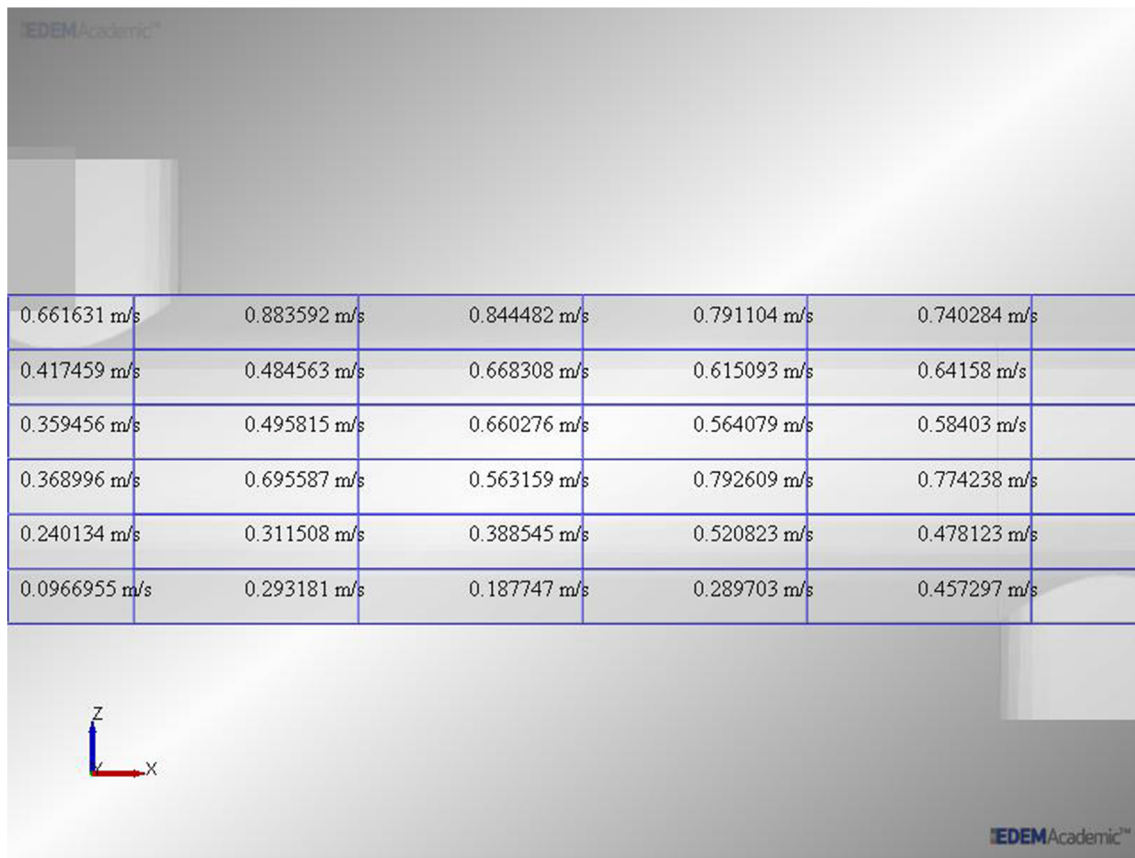| 0.661631 m/s | 0.883592 m/s | 0.844482 m/s | 0.791104 m/s | 0.740284 m/s |
0.417459 m/s	0.484563 m/s	0.668308 m/s	0.615093 m/s	0.64158 m/s
0.359456 m/s	0.495815 m/s	0.660276 m/s	0.564079 m/s	0.58403 m/s
0.368996 m/s	0.695587 m/s	0.563159 m/s	0.792609 m/s	0.774238 m/s
0.240134 m/s	0.311508 m/s	0.388545 m/s	0.520823 m/s	0.478123 m/s
0.0966955 m/s	0.293181 m/s	0.187747 m/s	0.289703 m/s	0.457297 m/s

Fig. 12 Radial velocity

Controller Model

Total Flow Rate from Blender (Cascade PID Controller) The total flow rate from the blender is calculated through a cascade control scheme. The deviation from the set point of total flow rate is calculated as follows:

$$\text{error}_{m_{out}} = m_{out\_set} - m_{out} \tag{6}$$

The total flow rate at feeder inlet is calculated as follows:

$$F_{T\_set} = K_C^{m_{out}} \text{error}_{m_{out}} + \frac{1}{K_I^{m_{out}}} \int_0^t \text{error}_{m_{out}} \, dt$$

$$+ K_D^{m_{out}} \frac{d(\text{error}_{m_{out}})}{dt} \tag{7}$$

API Composition (PID Controller) The deviation from the set point of API composition is calculated:

$$\text{error}_{C_{API}} = C_{API\_set} - C_{API} \tag{8}$$

The actuator setting is calculated on the basis of the deviation from the set point, using a PID control law:

$$\text{Ratio}_{set} = K_C^{C_{API}} \text{error}_{C_{API}} + \frac{1}{\tau_I^{C_{API}}} \int_0^t \text{error}_{C_{API}} \, dt + K_D^{C_{API}} \frac{d(\text{error}_{C_{API}})}{dt} \tag{9}$$

Ratio Controller The ratio controller calculates the set point of API, excipient, and lubricant feeders as follows:

$$F_{API\_set} = \text{Ratio}_{set} \cdot F_{T\_set} \tag{10}$$

$$F_{Lubricant\_set} = X_{lub} \cdot F_{T\_set} \tag{11}$$

$$F_{Excipient\_set} = (1 - \text{Ratio}_{set} - X_{lub}) \cdot F_{T\_set} \tag{12}$$

The feeder flow rates are then controlled through slave PID controllers by manipulating the respective feeder rotational speeds. The API feeder rotational speed is calculated as follows:

$$\text{rpm}_{API} = K_C^{F_{API}} \text{error}_{F_{API}} + \frac{1}{K_I^{F_{API}}} \int_0^t \text{error}_{F_{API}} \, dt + K_D^{F_{API}} \frac{d(\text{error}_{F_{API}})}{dt} \tag{13}$$

Similarly, excipient and lubricant feeder rotational speeds have been calculated.

Continuous Granulation Process

Process Model

A 3D population balance models is used to represent the granulation processes, taking into account distributions in particle size, liquid content, and porosity.

$$\frac{\partial F(s,l,g,z)}{\partial t} - \frac{\partial}{\partial g}\left(F(s,l,g,z)\frac{\mathrm{d}g}{\mathrm{d}t}\right) - \frac{\partial}{\partial t}\left(F(s,l,g,z)\frac{\mathrm{d}l}{\mathrm{d}t}\right) - \frac{\partial}{\partial z}(F(s,l,g,z)v_z) =$$
$$\mathfrak{R}_{\mathrm{agg}}(s,l,g,z) \quad + \quad \mathfrak{R}_{\mathrm{break}}(s,l,g,z) \quad + \quad \dot{F}_{\mathrm{in}}(s,l,g,z) - \dot{F}_{\mathrm{out}}(s,l,g,z) \tag{14}$$

$$\frac{\partial F(s,l,g)}{\partial t} = \mathfrak{R}_{\mathrm{break}}(s,l,g) + \dot{F}_{\mathrm{in}}(s,l,g) - \dot{F}_{\mathrm{out}}(s,l,g) \tag{15}$$

$$\dot{F}_{\mathrm{out}}(s,l,g,z) = \frac{F(s,l,g,z)v_z}{\Delta z} \tag{16}$$

The consolidation rate is given in Eq. 17 as proposed by Verkoeijen et al., where c is an empirical coefficient, and $\varepsilon_{\min}$ represents the minimum particle porosity observed [47]. V represents the total volume of the particle.

Here, F represents the total number of particles with each set of attributes, and s, l, and g represent the volumes of solid, liquid, and gas per particle. The granulation model contains one additional particle attribute, the axial position of the particle, represented by z. $\mathfrak{R}_{\mathrm{agg}}$ and $\mathfrak{R}_{\mathrm{break}}$ represent the net changes in particle count due to aggregation and breakage, and $\dot{F}_{\mathrm{in}}$ and $\dot{F}_{\mathrm{out}}$ represent the inlet and outlet streams.

In the granulation model, the consolidation, liquid spray rate, and particle flow terms are represented by the terms on the left-hand side of Eq. 16, where v_z is the average axial particle velocity. This value was based on an experimental residence time distribution and was assumed to be proportional to the impeller speed. The outlet flow rate is also based on this velocity, as given in Eq. 16 [30].

$$\frac{\mathrm{d}g}{\mathrm{d}t} = -cV\frac{(1-\varepsilon_{\min})}{s}\left(l - \frac{\varepsilon_{\min}s}{1-\varepsilon_{\min}} + g\right) \tag{17}$$

The liquid addition rate, shown in Eq. 18, is based on the total spray rate, u, the binder concentration, c_{binder}, and the total solid volume in the liquid addition region, V_{solid}

$$\frac{\mathrm{d}l}{\mathrm{d}t} = \frac{u(1-c_{\mathrm{binder}})}{V_{\mathrm{solid}}} \tag{18}$$

The net aggregation rate is given by Eq. 19, where K_{agg} is the aggregation kernel.

$$\mathfrak{R}_{\mathrm{agg}}(s,l,g,z) = \frac{1}{2}\iiint_0^s {}_0^l {}_0^g K_{\mathrm{agg}}(s',l',g',s-s',l-l',g-g')F(s',l',g',z)$$
$$F(s-s',l-l',g-g',z)\mathrm{d}g'\mathrm{d}l'\mathrm{d}s' - F(s,l,g,z)\iiint_s^\infty {}_l^\infty {}_g^\infty K_{\mathrm{agg}}(s,l,g,s',l',g')F(s',l',g',z)\mathrm{d}g'\mathrm{d}l'\mathrm{d}s' \tag{19}$$

A liquid-dependent aggregation kernel was implemented, as presented by Madec et al. and shown in Eq. 20,

where β_0, $\propto$, and δ are adjustable constants [48]. LC is the percent by volume of liquid in the particle.

$$K_{\mathrm{agg}}(s,l,g,s',l',g') = \beta_0(V+V')\left[(\mathrm{LC}+\mathrm{LC}')^\propto\left(100 - \frac{\mathrm{LC}+\mathrm{LC}'}{2}\right)^\delta\right]^\alpha \tag{20}$$

Similarly, the net breakage rate is given by Eq. 21, where K_{break} is the breakage rate kernel and b is the breakage distribution function.

$$\mathfrak{R}_{\text{break}}(s,l,g,z) = \iiint_{slg}^{\infty \quad \infty \quad \infty} K_{\text{break}}(s',l',g')F(s',l',g',z)b(s',l',g',s,l,g)\mathrm{d}g', \mathrm{d}l'\mathrm{d}s' - K_{\text{break}}(s,l,g)F(s,l,g,z) \tag{21}$$

A shear-rate-dependent breakage kernel was used, as shown in Eq. 22 [49]. Here, P_1 and P_2 are adjustable parameters, and G_{shear} is the shear rate, which was assumed to be proportional to the impeller speed.

$$K_{\text{break}}(s,l,g) = P_1 G_{\text{shear}} V^{P_2} \tag{22}$$

A uniform breakage distribution function was used in the model, which assumes that all size classes are equally likely to form for fragment particles, as shown in Eq. 23, where i, j, and k are the indices corresponding to the parent particle bins in s, l, and g, respectively.

$$b(s',l',g',s,l,g) = \frac{2}{(i-1)(j-1)(k-1)} \tag{23}$$

The same breakage rate kernel and distribution were used for milling. However, the values of the adjustable constants were different.

Finally, the outlet flow rate of the mill was based on a simple screen model. Particles smaller than the screen aperture exited the mill at a rate proportional to the impeller speed, v_{imp}, as shown in Eq. 24, where a_{out} is an adjustable coefficient.

$$F_{\text{out}}^{\cdot}(s,l,g) = a_{\text{out}} F v_{\text{imp}} \tag{24}$$

The population balance equations were discretized to form a series of coupled ordinary differential equations. Seven bins were used in each internal dimension (s, l, and g), and a linear grid with respect to volume was used. The axial coordinate of the granulator was represented by four spatial compartments, with liquid addition occurring in the second compartment. The main phenomenon during the granulation process is change in size of the particles based on the aggregation and breakage kernels. Therefore, unlike mixing, this process is more sensitive to the discretization of the internal coordinates (or particle size) rather than the external coordinates (external space). Moreover, the granulator has been divided into four compartments so that there is a clear distinction between the liquid addition period and the wet massing period (as has been mentioned in the manuscript that the liquid is added in the second compartment). This has been previously verified with very good accuracy in the works of Barrasso et al. [30].

Controller Model

Average Granule Size (PID Controller) The deviation from the set point of average granule size is calculated:

$$\text{error}_d = d_{\text{out\_set}} - d_{\text{out\_set}} \tag{25}$$

The final actuator setting (binder flow rate) is calculated on the basis of the deviation from the set point, using a PID control law:

$$F_{\text{b}} = K_C^d \text{error}_d + \frac{1}{K_I^d}\int_0^{t_f} \text{error}_d \mathrm{d}t + K_D^d \frac{d(\text{error}_d)}{\mathrm{d}t} \tag{26}$$

Bulk Density (PID Controller) The deviation from the set point of throughput is calculated:

$$\text{error}_\rho = -(\rho_{\text{set}} - \rho) \tag{27}$$

Note that the negative sign is because of reverse control action.

The actuator setting is calculated on the basis of the deviation from the set point, using a PID control law:

$$\omega = K_C^\lambda \text{error}_\rho + \frac{1}{K_I^\rho}\int_0^{t_f} \text{error}_\rho \mathrm{d}t + K_D^\rho \frac{d(\text{error}_\rho)}{\mathrm{d}t} \tag{28}$$

Milling

The population balance model is characterized by the internal coordinates API volume (s_1), excipient volume (s_2), and gas volume (g) [3]:

$$\frac{\partial}{\partial t}F(s_1,s_2,g,t) = \mathfrak{R}_{\text{break}}(s_1,s_2,g,t); \quad \mathfrak{R}_{\text{break}}(s_1,s_2,g,t) = \mathfrak{R}_{\text{break}}^{\text{formation}} - \mathfrak{R}_{\text{break}}^{\text{depletion}}$$

$$\mathfrak{R}_{\text{break}}^{\text{formation}} = \int_{s_1}^{\infty}\int_{s_1}^{\infty}\int_{s_1}^{\infty} k_{\text{break}}(s_1',s_2',g')b(s_1,s_2,g,s_1',s_2',g') \times F(s_1',s_2',g',t)\mathrm{d}s_1',\mathrm{d}s_2',\mathrm{d}g'$$

$$\mathfrak{R}_{\text{break}}^{\text{depletion}} = k_{\text{break}}(s_1,s_2,g)F(s_1,s_2,g,t) \tag{29}$$

Similar to the mixing model, density function $F(s_1,s_2,g,t)$ represents the number of moles of particles of API, excipient, and gas. Here, $\mathfrak{R}_{\text{break}}$ is the breakage rate, which is described by the difference between the rate of formation of new daughter particles and the rate of depletion of the original particle. In Eq. 29, the breakage rate is described by the breakage function (b) and the breakage kernel (k_{break}). As an initial condition, the mean particle size of the material that enters the mill is set to a really large value, resembling the size of broken ribbons.

The breakage kernel used in this study was a modified kernel based on the work by Matsoukas et al., where k_{break} has a size and composition (c_1, c_2) dependency, where different weights are assigned to the different components in order to introduce composition asymmetry in the model [50]. The current kernel in the literature is symmetrical, and as a result, deviations in the API composition from the desired value cannot be observed. The outputs of the PBM are particle size (d_{50}), bulk density ($\rho_{\text{bulk\_out}}$), and API composition (C_{API}), which are defined as follows:

$$d_{50}(t) = \left[\frac{6(s_1(t) + s_2(t) + g(t))}{\pi}\right]^{1/3}$$

$$\rho_{\text{bulk\_out}}(t) = \frac{\text{Mass of Solid}(t)}{\text{Total Volume}(t)} \tag{30}$$

$$C_{\text{API}}(t) = \frac{\sum \dfrac{F(t)s_1(t)}{(s_1(t) + s_2(t))}}{\sum F(t)}$$

Note that in this model, the evolution of the average particle diameter is tracked for all particle size ranges (i.e., fines, product, and oversized particles).

Hoppers

A hopper model is previously described in Singh et al. [18]. No variables are controlled in the hopper.

Tablet Press

The model of tablet pressing process is previously reported in Singh et al. [18]. The tablet compression model is adapted from Kawakita and Ludde [31] while the tablet hardness model is adapted from Kuentz and Leuenberger [51]. This model has been integrated with the flowsheet model of the continuous tablet manufacturing process via wet granulation and simulated in gPROMS. The control system has been then added to the model as described below.

Tablet Weight (Cascade PID Controller)

The deviation from the set point of tablet weight is calculated:

$$\text{error}_M = M_{\text{set}} - M \tag{31}$$

The set point for the slave controller (for the pre-compression pressure) is calculated on the basis of the deviation from the set point of tablet weight, using a PID control law:

$$C\_P_{\text{pre\_set}} = K_C^M \text{error}_M + \frac{1}{K_I^M}\int_0^t \text{error}_M \mathrm{d}t$$

$$+ K_D^M \frac{d(\text{error}_M)}{\mathrm{d}t} \tag{32}$$

The deviation from the set point of the pre-compression pressure is calculated as follows:

$$\text{error}_{C\_P_{\text{pre}}} = C\_P_{\text{pre\_set}} - C\_P_{\text{pre}} \tag{33}$$

The final actuator setting (feed volume) is calculated on the basis of the deviation from the set point, using a PID control law:

$$L_{\text{punch\_displ}} = K_C^{\text{main}} \text{error}_{C\_P_{\text{main}}} + \frac{1}{K_I^{\text{main}}}\int_0^t \text{error}_{C\_P_{\text{main}}} \mathrm{d}t + K_D^{\text{main}}\frac{d(\text{error}_{C\_P_{\text{main}}})}{\mathrm{d}t} \tag{34}$$

Tablet Hardness (Cascade PID Controller)

The deviation from the set point of tablet hardness is calculated:

$$\text{error}_H = H_{\text{set}} - H \tag{35}$$

H_{set} is calculated in "Dissolution Model" based on error in dissolution. The set point for the slave controller (for main-compression pressure) is calculated on the basis of the deviation from the set point of tablet hardness, using a PID control law:

$$C\_P_{\text{main\_set}} = K_C^H \text{error}_H + \frac{1}{\tau_I^H}\int_0^t \text{error}_H \mathrm{d}t$$

$$+ K_D^H \frac{d(\text{error}_H)}{\mathrm{d}t} \tag{36}$$

The deviation from the set point of the main-compression pressure is calculated as follows:

$$\text{error}_{C\_P_{\text{main}}} = C\_P_{\text{main\_set}} - C\_P_{\text{main}} \tag{37}$$

The final actuator setting (punch displacement) is calculated on the basis of the deviation from the set point, using a PID control law:

$$V_{\text{m}} = K_{\text{C}}^{\text{pre}}\text{error}_{C\_P_{\text{pre}}} + \frac{1}{\tau_{\text{I}}^{\text{pre}}} \int_0^t \text{error}_{C\_P_{\text{pre}}}\,\mathrm{d}t + K_{\text{D}}^{\text{pre}}\frac{d\left(\text{error}_{C\_P_{\text{pre}}}\right)}{\mathrm{d}t} \tag{38}$$

Dissolution Model

The details of the dissolution model are available in the scientific literatures [18, 32]. This model has been integrated with the flowsheet model, and the control system has been implemented as below.

The deviation from the set point of tablet dissolution is calculated:

$$\text{error}_{\text{des}} = \text{des}(t_{30})_{\text{set}} - \text{des}(t_{30}) \tag{39}$$

The set point for the slave controller (for hardness) is calculated on the basis of the deviation from the set point of tablet hardness, using a PID control law:

$$H_{\text{set}} = K_{\text{C}}^{\text{des}}\text{error}_{\text{des}} + \frac{1}{\tau_{\text{I}}^{\text{des}}} \int_0^t \text{error}_{\text{des}}\,\mathrm{d}t$$
$$+ K_{\text{D}}^{\text{des}}\frac{d(\text{error}_{\text{des}})}{\mathrm{d}t} \tag{40}$$

H_{set} is used in "Tablet Hardness (Cascade PID Controller)" for hardness control.

References

1. Singh R, Boukouvala F, Jayjock E, Ramachandran R, Ierapetritou M, Muzzio F. Flexible multipurpose continuous processing of pharmaceutical tablet manufacturing process, GMP news, European Compliance Academic (ECE). 2012b. http://www.gmpcompliance.org/ecanl_503_0_news_3268_7248_n.html. Accessed 1 Jul 2013.
2. Salman AD, Reynolds GK, Tan HS, Gabbott I, Hounslow MJ. Handbook of powder technology, Chapter 21: Breakage in granulation, 2007;11:979–1040.
3. Boukouvala F, Niotis V, Ramachandran R, Muzzio F, Ierapetritou M. An integrated approach for dynamic flowsheet modeling and sensitivity analysis of a continuous tablet manufacturing process: an integrated approach. Comput Chem Eng. 2012;42:30–47.
4. Boukouvala F, Ramachandran R, Vanarase A, Muzzio FJ, Ierapetritou M. Computer aided design and analysis of continuous pharmaceutical manufacturing processes. Comput Aided Chem Eng. 2011;29:216–20.
5. Keleb E, Vermeire A, Vervaet C, Remon J. Twin screw granulation as a simple and efficient tool for continuous wet granulation. Int J Pharm. 2004;273(12):183–94.
6. Vervaet C, Remon JP. Continuous granulation in the pharmaceutical industry. Chem Eng Sci. 2005;60(14):3949–57.
7. Singh R, Gernaey KV, Gani R. ICAS-PAT: a software for design, analysis & validation of PAT systems. Comput Chem Eng. 2010;34(7):1108–36.
8. Hsu S, Reklaitis GV, Venkatasubramanian V. Modeling and control of roller compaction for pharmaceutical manufacturing. Part I: Process dynamics and control framework. J Pharm Innov. 2010;5:14–23.
9. Hsu S, Reklaitis GV, Venkatasubramanian V. Modeling and control of roller compaction for pharmaceutical manufacturing. Part II: Control and system design. J Pharm Innov. 2010;5:24–36.
10. Ramachandran R, Chaudhury A. Model-based design and control of continuous drum granulation processes. Chem Eng Res Des. 2011;90(8):1063–73.
11. Burggraeve A, Tavares da Silva A, Van den Kerkhof T, Hellings M, Vervaet C, Remon JP, et al. Development of a fluid bed granulation process control strategy based on real-time process and product measurements. Talanta. 2012;100:293–302.
12. Bardin M, Knight PC, Seville JPK. On control of particle size distribution in granulation using high-shear mixers. Powder Technol. 2004;140(3):169–75.
13. Sanders CFW, Hounslow MJ, Doyle III FJ. Identification of models for control of wet granulation. Powder Technol. 2009;188(3):255–63.
14. Long CE, Polisetty PK, Gatzke EP. Deterministic global optimization for nonlinear model predictive control of hybrid dynamic systems. Int J Robust Nonlinear Control. 2007;17:1232–50.
15. Gatzke EP, Doyle III FJ. Model predictive control of a granulation system using soft output constraints and prioritized control objectives. Powder Technol. 2001;121(2–3):149–58.
16. Pottmann M, Ogunnaike BA, Adetayo AA, Ennis BJ. Model-based control of a granulation system. Powder Technol. 2000;108(2–3):192–201.
17. Ramachandran R, Arjunan J, Chaudhury A, Ierapetritou M. Model-based control loop performance assessment of a continuous direct compaction pharmaceutical processes. J Pharm Innov. 2012;6(3):249–63.
18. Singh R, Ierapetritou M, Ramachandran R. System-wide hybrid model predictive control of a continuous pharmaceutical tablet manufacturing process via direct compaction. Eur J Pharm Biopharm. 2013;85:1164–82.
19. Singh R, Godfrey A, Gregertsen B, Muller F, Gernaey KV, Gani R, et al. Systematic substrate adoption methodology (SAM) for future flexible, generic pharmaceutical production processes. Comput Chem Eng. 2013;58:344–368.
20. Boukouvala F, Chaudhury A, Sen M, Zhou R, Mioduszewski L, Ierapetritou MG, et al. Computer-aided flowsheet simulation of a pharmaceutical tablet manufacturing process incorporating wet granulation. J Pharm Innov. 2013;8:11–27.
21. Vanarase A, Muzzio FJ. Effect of operating conditions and design parameters in a continuous powder mixer. Powder Technol. 2011;208:26–36.
22. Portillo PM, Vanarase A, Ingram A, Seville JK, Ierapetritou MG, Muzzio FJ. Investigation of the effect of impeller rotation rate, powder flow rate, and cohesion on powder flow behavior in a continuous blender using PEPT. Chem Eng Sci. 2010;65:5658–68.
23. Vanarase A, Alcal M, Rozo J, Muzzio F, Romaach R. Real-time monitoring of drug concentration in a continuous powder mixing process using NIR spectroscopy. Chem Eng Sci. 2010;65(21):5728–33.

24. Vanarase A, Gao Y, Muzzio FJ, Ierapetritou MG. Characterizing continuous powder mixing using residence time distribution. Chem Eng Sci. 2011;66(3):417–25.

25. Ramachandran R, Chaudhury A. Model-based design and control of continuous drum granulation processes. Chem Eng Res Des. 2012;90(8):1063–73.

26. Sen M, Ramachandran R. A multi-dimensional population balance model approach to continuous powder mixing processes. Adv Powder Technol. 2012;24(1):51–9.

27. Sen M, Dubey A, Singh R, Ramachandran R. Mathematical development and comparison of a hybrid PBM-DEM description of a continuous powder mixing process. J Powder Technol 2012a. doi:10.1155/2013/843784.

28. Sen M, Singh R, Vanarase A, John J, Ramachandran R. Multi-dimensional population balance modeling and experimental validation of continuous powder mixing processes. Chem Eng Sci. 2012;80:349–60.

29. Barrasso D, Ramachandran R. A comparison of model order reduction techniques for a four-dimensional population balance model describing multi-component wet granulation processes. Chem Eng Sci. 2012;80:380–92.

30. Barrasso D, Walia S, Ramachandran R. Multi-component population balance modeling of continuous granulation processes: a parametric study and comparison with experimental trends. Powder Technol. 2013;241:85–97.

31. Kawakita K, Ludde KH. Some considerations on powder compression equations. Powder Technol. 1971;4:61–8.

32. Kimber JA, Kazarian SG, Stepánek F. Microstructure-based mathematical modelling and spectroscopic imaging of tablet dissolution. Comput Chem Eng. 2011;35:1328–39.

33. Seborg DE, Edgar TF, Mellichamp DA. Process dynamics and control. 2nd ed. New York: Wiley; 2004.

34. Singh R, Gernaey KV, Gani R. Model-based computer-aided framework for design of process monitoring and analysis systems. Comput Chem Eng. 2009;33(1):22–42.

35. Bristol E. On a new measure of interaction for multivariable process control. IEEE Trans Autom Control. 1966;11(1):133,134.

36. Blanco M, Alcalá M. Content uniformity and tablet hardness testing of intact pharmaceutical tablets by near infrared spectroscopy: a contribution to process analytical technologies. Anal Chim Acta. 2006;557:353–9.

37. Huang Z, Wang B, Li H. An intelligent measurement system for powder flowrate measurement in pneumatic conveying system. IEEE Trans Instrum Meas. 2002;51(4):700–3.

38. Prats-Montalbán JM, Jerez-Rozo JI, Romañach RJ, Ferrer A. MIA and NIR chemical imaging for pharmaceutical product characterization. Chemometr Intell Lab. 2012;117:240–9.

39. Roggo Y, Jent N, Edmond A, Chalus P, Ulmschneider M. Characterizing process effects on pharmaceutical solid forms using near-infrared spectroscopy and infrared imaging. Eur J Pharm Biopharm. 2005;61:100–10.

40. Singh R, Gernaey KV, Gani R. An ontological knowledge based system for selection of process monitoring and analysis tools. Comput Chem Eng. 2010;34(7):1137–54.

41. Sorokin LM, Gugnyak AB. A method of measuring powder flow rates. Powder Metall Met Ceram. 1973;12(12):1015–6. doi:10.1007/BF00791750.

42. Blevins T, Wojsznis, WK, Nixon M. Advanced control foundation: tools, techniques and applications. Research Triangle Park: International Society of Automation; 2013. ISBN: 978-1-937560-55-3.

43. Pawar P, Sullivan M, Heaps D, King E, Wang Y, Dendamrongvit W, Cuitino A, Muzzio FJ. Measurement of the effect of total shear and compaction force on tablet properties using terahertz pulsed spectroscopy: towards the prediction of dissolution rate. AIChE annual meeting, 404d, San Francisco, CA, 3–8 November, 2013.

44. El Hagrasy AS, Cruise P, Jones I, Litster JD. In-line size monitoring of a twin screw granulation process using high-speed imaging. J Pharm Innov. 2013;8(2):90–8.

45. Ziegler JG, Nichols B. Optimum settings for automatic controllers. Trans ASME. 1942;64:759–65.

46. Ogunnaike BA, Ray WH. Process dynamics, modeling, and control. New York: Oxford University Press; 1994.

47. Verkoeijen D, Pouw GA, Meesters GMH, Scarlett B. Population balances for particulate processes—a volume approach. Chem Eng Sci. 2002;57(12):2287–303.

48. Madec L, Falk L, Plasari E. Modelling of the agglomeration in suspension process with multidimensional kernels. Powder Technol. 2003;130(13):147–53.

49. Pandya J, Spielman L. Floc breakage in agitated suspensions: effect of agitation rate. Chem Eng Sci. 1983;38(12):1983–92.

50. Matsoukas T, Kim T, Lee K. Bicomponent aggregation with composition dependent rates and the approach to well-mixed state. Chem Eng Sci. 2009;64(4):787–99.

51. Kuentz M, Leuenberger H. A new model for the hardness of a compacted particle system, applied to tablets of pharmaceutical polymers. Powder Technol. 2000;111:143–5.